

# Journal of Materials Chemistry A

Accepted Manuscript



This is an *Accepted Manuscript*, which has been through the Royal Society of Chemistry peer review process and has been accepted for publication.

*Accepted Manuscripts* are published online shortly after acceptance, before technical editing, formatting and proof reading. Using this free service, authors can make their results available to the community, in citable form, before we publish the edited article. We will replace this *Accepted Manuscript* with the edited and formatted *Advance Article* as soon as it is available.

You can find more information about *Accepted Manuscripts* in the [Information for Authors](#).

Please note that technical editing may introduce minor changes to the text and/or graphics, which may alter content. The journal's standard [Terms & Conditions](#) and the [Ethical guidelines](#) still apply. In no event shall the Royal Society of Chemistry be held responsible for any errors or omissions in this *Accepted Manuscript* or any consequences arising from the use of any information it contains.



## Solution-Processed n-Doped Fullerene Cathode Interfacial Layer for Efficient and Stable Large-Area Perovskite Solar Cells

Chih-Yu Chang,<sup>\*a</sup> Wen-Kuan Huang,<sup>a</sup> Yu-Chia Chang,<sup>a</sup> Kuan-Ting Lee<sup>a</sup> and Chin-Ti Chen<sup>\*b</sup>

Received 00th January 20xx,  
Accepted 00th January 20xx

DOI: 10.1039/x0xx00000x

www.rsc.org/

A novel solution-processed cetyltrimethylammonium bromide (CTAB)-doped [6,6]-phenyl-C<sub>61</sub>-butyric acid methyl ester (PC<sub>61</sub>BM) film prepared by an extremely facile method is demonstrated as an effective cathode interfacial layer for perovskite solar cells (PSCs). Our results indicate that efficient doping takes place via anion-induced electron transfer between the bromide anions (Br<sup>-</sup>) on CTAB and PC<sub>61</sub>BM in the solid state, leading to a dramatic increase in electrical conductivity by more than five orders of magnitude. In addition, CTAB-doped PC<sub>61</sub>BM layer is capable of turning a more air-stable, high work-function (WF) Ag layer into efficient low WF electrode as a result of the formation of favorable interfacial dipoles between Ag and the active layer. These characteristics enable CTAB-doped PC<sub>61</sub>BM layer to function as both an electron transport layer and a cathode buffer layer (CBL) in PSCs, thus simplifying manufacturing process. This doped layer also exerts multi-positive effects for the use in PSCs, including efficient interfacial charge transfer ability, superior charge selectivity, good film coverage on the perovskite layer, relative weak thickness-dependent performance property, general applicability to different perovskite materials, and good ambient stability. With this n-doped PC<sub>61</sub>BM layer, the device delivers a high power conversion efficiency (PCE) up to 17.11%, which is superior to those of the devices with undoped PC<sub>61</sub>BM layer (2.15%) and state-of-the-art CBL ZnO nanoparticles (10.45%). The application of CTAB-doped PC<sub>61</sub>BM layer in large-area solar cells (active area = 1.2 cm<sup>2</sup>) is also demonstrated, and a remarkable PCE of 15.42% is achieved, which represents one of the highest PCE values for PSCs with similar active area. More significantly, the resulting devices possess good ambient stability without the need of rigorous encapsulation.

### Introduction

Hybrid organic–inorganic lead halide perovskite solar cells (PSCs) have recently emerged at the forefront of next-generation photovoltaic technology due to their potential for cost-effective manufacturing, light weight, and mechanical flexibility.<sup>1–4</sup> The most widely studied perovskite material is methylammonium lead iodide (MAPbI<sub>3</sub>), while formamidinium lead iodide (FAPbI<sub>3</sub>) has gained much attention recently because of its superior light-harvesting abilities. To date, the development of PSCs with planar heterojunction structure have suppressed a power conversion efficiency (PCE) of 19%,<sup>4–6</sup> thanks to significant progress made in the improvement of perovskite thin film quality and engineering the interface properties between the active layer and the electrode. Ideally, the work-function (WF) of the cathode and anode should be aligned with the energy of the photo-excited quasi-Fermi levels of active layer to ensure ohmic contact for maximizing achievable open-circuit voltage ( $V_{oc}$ ) and minimizing energy barrier for charge extraction without causing excessive interface recombination.<sup>1–4, 7</sup>

A basic planar heterojunction PSC device is the sandwich of light absorbing perovskite active layer between the hole transport layer (HTL) and electron transport layer (ETL) that are in contact with their corresponding electrodes. Among various device architectures utilized in planar heterojunction PSCs, the inverted architecture with a configuration of substrate/anode/HTL/perovskite/ETL/cathode has drawn much attention due to their low processing temperature and potential for use in plastic flexible devices.<sup>8–12</sup> A typically inverted device comprises indium tin oxide (ITO)-coated glass/poly(3,4-ethylenedioxythiophene):poly(styrenesulfonate) (PEDOT:PSS)/perovskite/[6,6]-phenyl-C<sub>61</sub>-butyric acid methyl ester (PC<sub>61</sub>BM)/cathode. Currently, low WF metals such as Al (~4.1 eV) or Ca (~2.9 eV) are often used as cathode electrodes to ensure efficient electron extraction.<sup>9–11</sup> Nevertheless, these low-work-function metals are vulnerable to oxidation in ambient environment, leading to poor device stability. Although the use of more environmental stable high WF metals such as Au (~5.1 eV) or Ag (~4.7 eV) as cathode is highly desirable, the mismatch between the WF of these metals and the lowest unoccupied molecular orbital (LUMO) level of PC<sub>61</sub>BM (~4.1 eV) ETL generally deteriorates the device performance.<sup>13–17</sup> To circumvent this problem, an effective strategy is to incorporate an additional cathode buffer layer (CBL) between PC<sub>61</sub>BM ETL and high WF cathode. Several solution-processed CBL materials, such as metal oxides or cationic quaternary ammonium-based molecules, have been applied to improve the contact properties

<sup>a</sup> Department of Materials Science and Engineering, Feng Chia University, Taichung, Taiwan 40724, R.O.C. (E-mail: changcyu@fcu.edu.tw)

<sup>b</sup> Institute of Chemistry, Academia Sinica, Taipei, Taiwan 11529, R.O.C. (E-mail: chintchen@gate.sinica.edu.tw)

Electronic Supplementary Information (ESI) available: [details of any supplementary information available should be included here]. See DOI: 10.1039/x0xx00000x

and consequently enhance the device performance.<sup>7, 8, 13-17</sup> These CBL materials have good solubility in polar solvents that enable multilayer film deposition without destroying underlying PC<sub>61</sub>BM layer. In addition, they can generally induce favorable interfacial dipole to lower the WF of the electrode and consequently a better energy level alignment at PC<sub>61</sub>BM–electrode interface, leading to significantly improved device performance. Despite these perceived advantages, the incorporation of these CBLs certainly increases the fabrication complexity and reduce the reproducibility due to the requirements of additional coating steps and accurate layer thicknesses. Given that an effective CBL must be thin, typically in the range of 5–25 nm,<sup>7, 13-16</sup> it is therefore particularly challenging to deposit uniform and pinhole-free CBL on the rough PC<sub>61</sub>BM/perovskite surface. The insufficient CBL film coverage can create electrical shunting paths and thus leading to deteriorated device performance.<sup>9, 14, 17</sup>

This study aims to overcome the above-mentioned challenges by developing a novel n-doped PC<sub>61</sub>BM that is capable of serving as both an ETL and a CBL in PSCs with more environmentally stable high WF Ag as the cathode layer. The device configuration used herein is glass/ITO/PEDOT:PSS/perovskite/n-doped PC<sub>61</sub>BM/Ag, as depicted in Fig. 1a. To the best of our knowledge, this is the first demonstration of n-doped fullerene layer that can function as both ETL and CBL in PSCs. Previous studies have shown that alkyl ammonium-based surfactants are effective n-type dopants that can cause n-doping of fullerenes via anion-induced electron transfer. In our approach, we incorporate commercial available cetyltrimethylammonium bromide (CTAB) as the n-type dopant into PC<sub>61</sub>BM host material (see Fig. 1a for the chemical structures). The long alkyl chain on CTAB surfactant can ensure high solubility in various organic solvents and good stability, whereas quaternary ammonium cations can induce the formation of favorable interfacial dipoles to lower the WF of Ag electrode. Our results also confirm that efficient doping occurs via anion-induced electron transfer between the bromide anions (Br<sup>-</sup>) on CTAB and PC<sub>61</sub>BM in the solid state, leading to a dramatic increase in electrical conductivity (by more than five orders of magnitude). In addition, this doped PC<sub>61</sub>BM layer delivers several remarkable features for the use in PSCs, including efficient interfacial charge transfer ability, superior charge selectivity, good film coverage on the perovskite layer, relative weak thickness-dependent performance property, reasonable ambient stability, and general applicability to different perovskite systems (MAPbI<sub>3</sub> and FAPbI<sub>3</sub>). With these desired properties, PSCs deliver a PCE up to 17.11% with high reproducibility, greatly outperforming the devices with undoped PC<sub>61</sub>BM film and state-of-the-art CBL ZnO nanoparticles (NPs). Importantly, the resulting devices possess good ambient stability without the need of rigorous encapsulation. More significantly, the applicability of this approach in large-area devices (1.2 cm<sup>2</sup>) is also demonstrated, and a remarkable PCE up to 15.42% is achieved. This work demonstrates an effective approach to improve the performance and stability of PSCs through facile chemical doping.

## Results and discussion

To confirm efficient electron transfer from the anions of CTAB to PC<sub>61</sub>BM, the electron paramagnetic resonance (EPR) spectra of PC<sub>61</sub>BM films with and without adding CTAB dopant were recorded at room temperature (Fig. 1b). The films were deposited on the walls of quartz EPR tubes by evaporation of solvent (chloroform) under vacuum at 60 °C. As shown in Fig. 1b, no appreciable paramagnetic signal was observed for the undoped film, indicating its semiconducting nature. In contrast, the doped film revealed a strong paramagnetic signal, suggesting the formation of n-doped fullerene radical anions. We then studied the influence of CTAB doping on the electrical properties of PC<sub>61</sub>BM film. The electrical conductivities of PC<sub>61</sub>BM film at varied dopant concentration were measured by the four-point probe technique, and the results were depicted in Fig. 1c. As the concentration of CTAB increased, the conductivity first increased dramatically. As shown in Fig. 1c, the conductivity increased from  $2.1 \times 10^{-8}$  S cm<sup>-1</sup> (undoped film) to a maximum of  $4.8 \times 10^{-3}$  S cm<sup>-1</sup> (doping concentration = 10 mol%), which is comparable to those of the other organic conducting materials such as PEDOT:PSS ( $10^{-3}$  S cm<sup>-1</sup> for Clevious P Al4083) and anionic conjugated polyelectrolyte ( $\sim 1.5 \times 10^{-3}$  S cm<sup>-1</sup>).<sup>18, 19</sup> When the doping concentrations were further increased beyond 10 mol%, however, the conductivity decreased gradually (Fig. 1c). This deterioration could be ascribed to the tendency of excess CTAB-caused aggregation and will be discussed later. In addition to the reasonable conductivity, we observed that the doped PC<sub>61</sub>BM film (doping concentration = 10 mol%) possessed good ambient stability: electrical conductivity remained fairly high ( $>10^{-3}$  S cm<sup>-1</sup>) upon exposure to ambient air (30 °C,  $\sim 60\%$  relative humidity) for more than 110 hr (Fig. 1d). This result suggests that negative charge carriers within the doped film are not quenched significantly by ambient oxygen and moisture, which may be associated with the hydrophobic nature of PC<sub>61</sub>BM film.

To gain more insight into the morphological alteration of PC<sub>61</sub>BM-coated MAPbI<sub>3</sub> perovskite films, atomic force microscopy (AFM) measurements were carried out in tapping mode. The obtained topography images of 5 μm × 5 μm scans of the films were depicted in Fig. 2. The MAPbI<sub>3</sub> perovskite film was prepared by two-step sequential solution deposition, and its detailed characterization can be found in our previous studies.<sup>15, 17</sup> The pristine perovskite sample (i.e., without PC<sub>61</sub>BM layer) revealed an inhomogeneous and incomplete film morphology, with a root mean square (rms) roughness of  $\sim 25.9$  nm (Electronic supplementary information (ESI) Fig. S1). The introduction of undoped PC<sub>61</sub>BM layer, however, can only partially fill the voids in the underlying layers, as the PC<sub>61</sub>BM-coated sample still revealed a void-presented morphology with a high root-mean-square (rms) surface roughness of 3.9 nm (Fig. 2a). When mixing CTAB in chloroform solution of PC<sub>61</sub>BM, we have noticed the solution became considerably viscous. This can be ascribed to the coulombic interaction between PC<sub>61</sub>BM radical anion and cetyltrimethylammonium cation, of which floppy hydrocarbon chain of cetyl group limits the fluidity of such ion pair in chloroform. The combination of ion pair

interaction and long floppy cetyl group reduces the aggregation of PC<sub>61</sub>BM and facilitates the coverage of PC<sub>61</sub>BM film onto the perovskite layer. As shown in Fig. 2b and c, PC<sub>61</sub>BM films with CTAB doping concentration below 10 mol% revealed uniform and void-free morphology, suggesting that the addition of CTAB dopant could facilitate the formation of uniform PC<sub>61</sub>BM film. We also noticed that these films were quite smooth (rms roughness ~1.6 nm) with no obvious phase separation, indicating high miscibility between PC<sub>61</sub>BM and CTAB. Further increases in the doping concentration of CTAB beyond 10 mol% revealed a greater surface roughness (rms roughness ~3.4 nm) with more pronounced phase-separated domains (Fig. 2d and e). This would hinder efficient charge transport between neighbouring domains and thus lead to low conductivity, as depicted in Fig. 1c.

In order to investigate if doped film could contribute to efficient charge transfer at the perovskite/PC<sub>61</sub>BM interface, we carried out steady-state photoluminescence (PL) and time-resolved PL decay measurement. The PL properties of glass/MAPbI<sub>3</sub>, glass/MAPbI<sub>3</sub>/PC<sub>61</sub>BM, and glass/MAPbI<sub>3</sub>/CTAB-doped PC<sub>61</sub>BM (doping concentration = 10 mol%) were measured under excitation at a wavelength of 450 nm, and PL emission was collected from the glass substrate side. As shown in Fig. 3a, the significant PL quenching effect was observed when the perovskite layer formed a contact with either undoped PC<sub>61</sub>BM or doped PC<sub>61</sub>BM layer. The quenching of PL intensity is consistent with previous studies and is generally ascribed to charge transfer at the perovskite/fullerene interface.<sup>10, 20-22</sup> For undoped PC<sub>61</sub>BM-coated sample, ~4% PL intensity was retained, while nearly all intensity was quenched for doped PC<sub>61</sub>BM-coated sample (Fig. 3a), suggesting that charge carrier transfer at the perovskite/doped PC<sub>61</sub>BM interface was more efficient than the perovskite/undoped PC<sub>61</sub>BM interface, presumably due to superior film quality of doped PC<sub>61</sub>BM on the perovskite layer as discussed previously (Fig. 2). Efficient charge transfer was also manifest in a reduction of the PL lifetimes when PC<sub>61</sub>BM layer was present. The glass/MAPbI<sub>3</sub> sample exhibited a long average lifetime of 11.8 ns, which is comparable to the lifetimes of MAPbI<sub>3</sub> perovskite reported previously.<sup>20, 21</sup> The average lifetime value for glass/MAPbI<sub>3</sub>/PC<sub>61</sub>BM and glass/MAPbI<sub>3</sub>/doped PC<sub>61</sub>BM sample was 0.65 and 0.32 ns, respectively (Fig. 3b). These results suggest that the introduction of CTAB-doped PC<sub>61</sub>BM layer facilitates efficient charge-carrier transfer at the interface, which can suppress the charge carrier recombination and enhance the charge generation and collection in the devices (as will be discussed later).

The effect of doping on the WF of Ag electrode was then investigated by ultraviolet photoelectron spectroscopy (UPS) measurement. As shown in Fig. 3c, the WF value of bare Ag electrode was determined to be 4.63 eV, which is very close to the reported values (~4.70 eV). When Ag electrode was modified with doped PC<sub>61</sub>BM film (10 mol% doping), the WF was effectively reduced to 3.81 eV. The low WF contact at the cathode interface provides better energy level matching with electron-accepting PC<sub>61</sub>BM layer and forms ohmic contact (Fig. 3d), which is preferable for efficient electron extraction as

described previously.<sup>1-3</sup> This effective WF modulation would be beneficial for improving the built-in potential in device thus contributes to high open-circuit voltage ( $V_{oc}$ ), as discussed later. The significant decrease in the WF via CTAB doping can be attributed to the formation of favorable interfacial dipole created by the strong interaction between the ammonium cations and Ag electrode surface, as several recent studies have demonstrated that the introduction of ammonium cations-based molecules at the cathode interface can induce interfacial dipoles toward the active layer that can significantly elevate the vacuum level of the cathode for efficient electron extraction.<sup>13-15</sup> It should be noted that the WF of Ag electrode modified with CTAB layer (i.e., without PC<sub>61</sub>BM) was 3.73 eV (Fig. 3c), which was nearly comparable to that of doped PC<sub>61</sub>BM-modified Ag layer (3.81 eV). These results indicate that CTAB-doped PC<sub>61</sub>BM layer is able to turn air-stable high WF Ag electrode into efficient low WF electrode.

The device performance with CTAB-doped PC<sub>61</sub>BM layer (doping concentration = 10 mol%) was then studied, and a control device with undoped PC<sub>61</sub>BM layer was also fabricated for comparison. The device configuration was glass substrate/ITO/PEDOT:PSS/MAPbI<sub>3</sub>/PC<sub>61</sub>BM (with and without CTAB doping)/Ag. The solar-to-electrical PCE were evaluated by recording the current-voltage ( $J-V$ ) characteristics under simulated AM 1.5 G conditions (intensity = 100 mWcm<sup>-2</sup>). The average values and the corresponding standard deviations of photovoltaic parameters including  $V_{oc}$ , short-circuit current density ( $J_{sc}$ ), fill factor (FF), and PCE were summarized in Table 1. The  $J-V$  characteristics of the best performing devices were also depicted in Fig. 4a, and the detailed photovoltaic parameters were listed in Table 1. For the control device employing undoped PC<sub>61</sub>BM layer (device A), an average PCE of 2.44% was attained, with  $J_{sc}$  of 15.04 mA cm<sup>-2</sup>,  $V_{oc}$  of 0.46 V, and FF of 35.57% (Table 1 and Fig. 4a). The poor device performance obtained for device A is consistent with previous findings that a large energy barrier exists between the LUMO level of PC<sub>61</sub>BM and the WF of Ag. When using CTAB-doped PC<sub>61</sub>BM film as cathode interfacial layer (device B), a substantial improvement in PCE (by ~6.2 fold) was demonstrated as a result of the simultaneously increased all the parameters. As shown in Table 1, device B exhibited an average PCE of 15.19%, with  $J_{sc}$  of 20.13 mA cm<sup>-2</sup>,  $V_{oc}$  of 1.0 V, and FF of 75.53%. In particular, the best performing device showed a PCE of 16.11%, with  $J_{sc}$  of 20.27 mA cm<sup>-2</sup>,  $V_{oc}$  of 1.01 V, and FF of 78.68% (Table 1 and Fig. 4a). In addition, device B showed a good stabilized power output: a stable value as high as 15.78% was observed (ESI Fig. S2). Note that the measured  $J_{sc}$  of device B agreed very well (within 10% error) with the  $J_{sc}$  values integrated from incident photon-to-current conversion efficiency (IPCE) spectra (Fig. 4b and ESI Fig. S3), which confirmed the accuracy of our reported PCE values. Considering that ZnO nanoparticles (NPs) film is commonly employed as CBL for perovskite solar cells,<sup>1, 10</sup> a device with ZnO NPs CBL was also fabricated for comparison (device C). Encouragingly, the optimized CTAB-doped PC<sub>61</sub>BM device greatly outperformed ZnO NPs-based device (maximum PCE: 16.11% vs. 10.23%), as shown in Table 1 and Fig. 4a. The inferior PCE of ZnO NPs-based device can be rationalized by the fact that

ZnO NPs film can only partially fill the voids in the underlying PC<sub>61</sub>BM/perovskite layers and consequently cause shunt leakage pathways and low device performance, as discussed in our previous study.<sup>17</sup> While this issue was absent in the case of CTAB-doped PC<sub>61</sub>BM layer, as evidenced by the highly uniform and void-free surface morphology (Fig. 2). In addition, it is generally accepted that the electrical coherence at the organic/inorganic interface is inferior to that at the organic/organic interface,<sup>7,23</sup> which could be another reason for the lower PCE of ZnO NPs CBL-based device. It should be noted that the photovoltaic performance of the device using CTAB as CBL (device D) was found to be inferior to that of doped device (Table 1 and Fig. 4a), presumably due to the insufficient CTAB film coverage, as can be seen from AFM topography image shown in ESI Fig. S4. These results clearly indicate the effectiveness of using CTAB-doped PC<sub>61</sub>BM film as the viable cathode interfacial layer in PSCs.

To check the reproducibility of the devices, a histogram of device performance obtained from 50 samples of device B was summarized in Fig. 4c. Importantly, more than 60% of the integrated devices delivered PCE above 15% with low standard deviation (Table 1 and Fig. 4c), indicating good reproducibility. This could be explained by superior coverage of CTAB-doped PC<sub>61</sub>BM film on the perovskite layer as depicted in Fig. 2. In addition, given that planar heterojunction PSCs have been shown to be prone to hysteresis, *J-V* characteristic of the device with doped PC<sub>61</sub>BM layer (device B) measured under different scan conditions was then analyzed. Encouragingly, we observed that our device exhibited photocurrent hysteresis-free *J-V* characteristics with different scanning directions and/or voltage sweep rates (Fig. 4d and e), which can be ascribed to effective passivation of trap states in the perovskite afforded by PC<sub>61</sub>BM capping layer.<sup>9,24</sup>

To gain deeper insight into the PCE improvement afforded by CTAB dopant, the series resistance ( $R_s$ ) and shunt resistance ( $R_{sh}$ ) of the devices were investigated. The  $R_s$  and  $R_{sh}$  are calculated from the inverse slope of the *J-V* characteristics under dark conditions close to 0 and 1 V, respectively. As shown in ESI Table S1 and Fig. 4f, compared to the device with undoped PC<sub>61</sub>BM layer (device A), the device with doped PC<sub>61</sub>BM layer (device B) exhibited lower series resistance and higher shunt resistance (i.e. less charge recombination and leakage current), indicating more effective charge selective contact. This improvement could be attributed to the combined positive effects afforded by CTAB-doped PC<sub>61</sub>BM layer, including enhanced electrical conductivity, superior film quality, and good WF tenability of Ag electrode, as we had discussed previously. These results elucidate that CTAB-doped PC<sub>61</sub>BM layer can provide interface modification superior to that of undoped film, ensuring efficient electron extraction and preventing undesirable electron-hole recombination between the active layer and Ag electrode.

Controlling the thickness of interfacial layer usually plays an important role for performance optimization of perovskite solar cells.<sup>7, 13-15</sup> Here the thickness effects of the undoped PC<sub>61</sub>BM and CTAB-doped PC<sub>61</sub>BM (doping concentration = 10 mol%) films on the PCEs of perovskite solar cells were investigated. For the devices with undoped PC<sub>61</sub>BM layer, a strong correlation

between the device performance and layer thickness was observed. The PCE rapidly declined from 3.03% to 2.11% when film thickness was increased from the optimal thickness of 60 nm to 80 nm (Table 2 and Fig. 5a). When employing doped PC<sub>61</sub>BM film as cathode interfacial layer, however, the device performance exhibited a more slowly decline with respect to the ones with undoped PC<sub>61</sub>BM layer (Table 2 and Fig. 5b). Even with a high-thickness of doped film (~120 nm), the device still remained a reasonable PCE of 13.18% (Table 2 and Fig. 5b). The diminished thickness-dependent performance property in the case of doped PC<sub>61</sub>BM layer could be ascribed to superior electrical conduction capability, as evidenced by the conductivities measurement shown in Fig. 1c. This thickness-insensitive property would be beneficial for mass production techniques, such as blade coating or inkjet printing.

The universality of this CTAB-doped PC<sub>61</sub>BM layer (doping concentration = 10 mol%) in PSCs was examined with FAPbI<sub>3</sub> perovskite layer, which is potentially superior to conventional MAPbI<sub>3</sub> as the light harvester because of the smaller bandgap.<sup>5, 25, 26</sup> The FAPbI<sub>3</sub> perovskite was prepared according to the reported procedure.<sup>5</sup> The formation of high purity FAPbI<sub>3</sub> perovskite film was confirmed by high resolution X-ray diffraction (XRD) analysis, as shown in ESI Fig. S5. The device fabrication procedure was the same as for MAPbI<sub>3</sub>-based devices, except that the active layer was replaced by FAPbI<sub>3</sub> (see experimental for details). The devices with undoped PC<sub>61</sub>BM layer and ZnO NPs CBL were also fabricated for comparison. The *J-V* characteristics of the best performing devices were shown in Fig. 6a, and the detailed photovoltaic parameters were summarized in Table 3. Very encouragingly, the device with doped PC<sub>61</sub>BM layer (device E) delivered a remarkable PCE of 17.11%, which was superior to those of the devices with ZnO CBL (device F; maximum PCE = 10.45%) and undoped PC<sub>61</sub>BM (device G; maximum PCE = 2.15%). In addition, a good stabilized power output was also observed for device E, delivering a stable PCE value as high as 16.80% (ESI Fig. S2). Note that the measured  $J_{sc}$  of device E agreed very well (within 10% error) with the  $J_{sc}$  value integrated from IPCE spectra (Fig. 4b and ESI Fig. S3), which confirmed the accuracy of our reported PCE value. It should be emphasized again that all key parameters of the device with doped PC<sub>61</sub>BM layer were highly reproducible with low standard deviation (Table 3). These results provide strong evidence of the general utility of CTAB-doped PC<sub>61</sub>BM layer in PSCs.

The device performance of PSCs is known to be limited by the active area. Most of the record efficiencies were reported for small active area devices (<1 cm<sup>2</sup>), and the PCEs are generally considerably lower for larger area devices.<sup>27</sup> To ensure large-area devices with both satisfactory PCE and good reproducibility, the development of appropriate interfacial layers remain highly desirable. Given that CTAB-doped PC<sub>61</sub>BM layer significantly improved the interface properties between the active layer and Ag electrode, its applicability in large-area PSCs was examined. The fabrication procedure and device structure was the same as for the small-area device (device E) except that the active area was increased from 0.12 to 1.2 cm<sup>2</sup>. As shown in Fig. 6b, the best performing device delivered a high PCE of 15.42%, with  $J_{sc}$  of

20.70 mA cm<sup>-2</sup>,  $V_{oc}$  of 1.03V, and FF of 72.34%. It should be noted that 15.42% PCE of the large-area device is among one of the highest reported values for PSCs with similar active area (1.0-1.2 cm<sup>2</sup>).<sup>27-29</sup> These remarkable results can be ascribed to the fact that CTAB-doped PC<sub>61</sub>BM layer exerts multiple positive effects on the device characteristics, including superior film quality, good charge selectivity, and reasonable electrical conductivity. Considering that organic-inorganic lead halide perovskite materials will decompose rapidly in the presence of moisture,<sup>30</sup> the shelf stability of large-area FAPbI<sub>3</sub>-based devices was also examined by monitoring the evolution of their PCEs as a function of time during storage under ambient conditions (30 °C, ~60% relative humidity). In our case, no extra package or encapsulation layer was used. Notably, after being exposed to ~360 hr, over 80% of the initial PCE could be retained for these devices (Fig. 6c). This might be associated with superior air stability afforded by ambient-stable Ag electrode and uniform coverage of CTAB-doped PC<sub>61</sub>BM layer, as discussed previously. In particular, we found that these devices remained quite stable in ambient atmosphere under continuous light illumination (intensity = 100 mW cm<sup>-2</sup>): more than 60% of the initial efficiency was retained over 120 hr continuous testing (Fig. 6c), demonstrating good stability of doped devices not only in ambient environment but also under continuous illumination. These results indicate high compatibility of CTAB-doped PC<sub>61</sub>BM layer with large scale processing, enabling the resulting devices to exhibit both high performance and good ambient stability.

## Conclusions

A facile and effective method to improve the performance and stability of PSCs is demonstrated by the in-corporation of solution-processed CTAB-doped PC<sub>61</sub>BM as the as both an ETL and a CBL. With this layer, the device exhibited a remarkable PCE up to 17.11% with high reproducibility (average PCE = 15.60%), greatly outperforming the devices with undoped PC<sub>61</sub>BM layer (2.15%) and the state-of-the-art CBL ZnO NPs (10.45%). In addition, the applicability of using this doped layer in large-area of 1.2 cm<sup>2</sup> PSCs is also demonstrated, and a record high PCE of 15.42% is achieved. More significantly, the resulting devices also possess good ambient stability. This work demonstrates a simple and effective strategy that enables significant improvement in performance and stability of large-area PSCs through facile chemical doping. The results also provide valuable insights into the development of solution-processed n-doped cathode interfacial layers in PSCs.

## Experimental

### Materials

Patterned ITO-coated glass substrates with a sheet resistance of 15 ohm sq<sup>-1</sup> were purchased from Ruilong Tech. PEDOT:PSS aqueous solution (CLEVIOS P VP Al 4083) was purchased from Heraeus. Methylammonium iodide (MAI; >99.5%) and formamidinium iodide (FAI; >99.5%) were purchased from Lumtec. PC<sub>61</sub>BM (>99.5%) was purchased from Solenne. For

preparation of lead iodide (PbI<sub>2</sub>) complex, 25 g PbI<sub>2</sub> was dissolved in anhydrous dimethylsulfoxide of 75 mL and toluene of 200 ml was then slowly added into the PbI<sub>2</sub> solution. The white precipitation was then filtered and dried in vacuum oven at 60 °C for 12 hr. Unless otherwise stated, all chemicals were purchased from Sigma-Aldrich and used as received.

### Synthesis of ZnO NPs:

ZnO NPs were synthesized by a solution-precipitation process according to literature procedures.<sup>31</sup> Briefly, zinc acetate dihydrate (2.95 g) was dissolved in methanol (125 mL) at room temperature. A potassium hydroxide solution (1.48 g in 65 mL methanol) was then added dropwise within 30 min and stirred for 3 hr at 65 °C. The cooled-down solution was then decanted and the precipitate washed twice with ethyl acetate and ethanol. Afterward, ethanol was added to disperse the precipitates and produce ZnO NPs solution.

### Solar cell fabrication

ITO-coated glass substrates were cleaned stepwise in detergent, water, acetone, and isopropyl alcohol under ultrasonication for 20 min each and subsequently pretreated by UV-ozone for 60 min. The PEDOT:PSS layer (25 nm) was spin-coated on ITO surface and then annealed at 120 °C for 15 min. The MAPbI<sub>3</sub> perovskite layer (~250 nm) was prepared following two-step solution deposition, as described in our previous work.<sup>15, 17</sup> Briefly, PbI<sub>2</sub> and MAI were dissolved into anhydrous dimethylformamide (DMF) and anhydrous 2-propanol with concentrations of 450 mg mL<sup>-1</sup> for PbI<sub>2</sub> and 40 mg mL<sup>-1</sup> for MAI, respectively. Both solutions and substrates were heated at 100 °C for 10 min before being used. The PbI<sub>2</sub> solution was spun on preheated substrate (5000 rpm for 40 sec) and then annealed at 70 °C for 10 min. The MAI solution was then spun on top of dried PbI<sub>2</sub> film (6000 rpm for 30 sec), followed by annealing at 100 °C for 2 hr. The FAPbI<sub>3</sub> perovskite layer (~380 nm) was prepared according to the reported procedure.<sup>5</sup> Briefly, the PbI<sub>2</sub> complex solution (1.3 M in anhydrous DMF) was spun on the substrate (3000 rpm for 30 sec). The FAI solution (0.465 M in anhydrous 2-propanol) was then spun on top of dried PbI<sub>2</sub> complex film (5000 rpm for 30 sec), followed by annealing at 150 °C for 10 min. Afterward, a solution consisting of 20 mg mL<sup>-1</sup> PC<sub>61</sub>BM with different doping ratio of CTAB in anhydrous chloroform was then spin-coated on top of the formed perovskite layers. The optimum thickness of PC<sub>61</sub>BM layer for MAPbI<sub>3</sub> and FAPbI<sub>3</sub> was 60 and 80 nm, respectively. The opaque Ag (150 nm) was then deposited from thermal evaporator under high vacuum (<10<sup>-6</sup> torr). Contributions to the  $J_{sc}$  from regions outside the active area were eliminated using illumination masks with aperture size of 0.12 cm<sup>2</sup> or 1.2 cm<sup>2</sup>.

### Characterization

The current-voltage characteristics of as-fabricated solar cells were measured under ambient using a Keithley 2400 source measurement unit. Unless otherwise stated, the scan rate was set at 0.15 V s<sup>-1</sup>. An Oriel xenon lamp (450 Watt) with an AM1.5 G filter was used as the solar simulator. A Hamamatsu silicon

solar cell (S1133) with a KG5 color filter, which is traced to the National Renewable Energy Laboratory (NREL), was used as the reference cell. To calibrate the light intensity of the solar simulator, the power of the xenon lamp was adjusted to make the  $J_{sc}$  of the reference cell under simulated sun light as high as it was under the calibration condition. IPCE spectra were measured using a lock-in amplifier with a current preamplifier under short-circuit conditions with illumination of monochromatic light from a 250 W quartz-halogen lamp (Osram) passing through a mono-chromator. The work functions of the electrodes were measured with a ULVAC-PHI PHI 5000 Versaprobe II X-ray photoelectron spectrometer employing a mono-chromatic focused Al-K $\alpha$  X-ray source and hemispherical analyzer. The EPR spectra were performed at room temperature using Bruker ELEXSYS E-580 EPR spectrometer. Sample solutions were added to EPR test tubes and then degassed with nitrogen to form films on the tube walls at room temperature under nitrogen atmosphere. Steady-state PL spectra were measured at room temperature by using a fluorescent spectrophotometer (Hitachi F-4600) with a 150W Xe lamp as an excitation source at 600 nm. Time-resolved PL decay spectra were recorded by a time-correlated single-photon counting system (Edinburgh Instruments FL920), and the excitation light pulse was provided using a picosecond diode laser at a wavelength of 450 nm, and the signal was monitored at  $\sim$ 770 nm. The PL lifetimes of the samples was calculated by fitting the experimental decay transient data to the single-exponential decay model. The surface morphology of the films was studied using the tapping mode AFM from Digital Instrument D3100CL. The electrical conductivities of the thin films were measured by using a four point probe setup with a source measurement unit (Keithley 2400).

## Acknowledgements

We thank the Ministry of Science and Technology (Grant MOST 04-2221-E-035-035 and 104-2119-M-009 -012) for support. We also appreciate the Precision Instrument Support Center of Feng Chia University for providing the fabrication and measurement facilities.

## Notes and references

- P. Gao, M. Gratzel and M. K. Nazeeruddin, *Energy Environ. Sci.*, 2014, **7**, 2448.
- H. S. Jung and N.-G. Park, *Small*, 2015, **11**, 10.
- O. Malinkiewicz, A. Yella, Y. H. Lee, G. M. Espallargas, M. Graetzel, M. K. Nazeeruddin and H. J. Bolink, *Nat. Photon.*, 2014, **8**, 128.
- H. Zhou, Q. Chen, G. Li, S. Luo, T.-b. Song, H.-S. Duan, Z. Hong, J. You, Y. Liu and Y. Yang, *Science*, 2014, **345**, 542.
- W. S. Yang, J. H. Noh, N. J. Jeon, Y. C. Kim, S. Ryu, J. Seo and S. I. Seok, *Science*, 2015, **348**, 1234.
- N. Ahn, D.-Y. Son, I.-H. Jang, S. M. Kang, M. Choi and N.-G. Park, *J. Am. Chem. Soc.*, 2015, **137**, 8696.
- C.-C. Chueh, C.-Z. Li and A. K. Y. Jen, *Energy Environ. Sci.*, 2015, **8**, 1160.
- P.-W. Liang, C.-Y. Liao, C.-C. Chueh, F. Zuo, S. T. Williams, X.-K. Xin, J. Lin and A. K. Y. Jen, *Adv. Mater.*, 2014, **26**, 3748.
- Q. Wang, Y. Shao, Q. Dong, Z. Xiao, Y. Yuan and J. Huang, *Energy Environ. Sci.*, 2014, **7**, 2359.
- J. You, Z. Hong, Y. Yang, Q. Chen, M. Cai, T.-B. Song, C.-C. Chen, S. Lu, Y. Liu, H. Zhou and Y. Yang, *ACS Nano*, 2014, **8**, 1674.
- A. T. Barrows, A. J. Pearson, C. K. Kwak, A. D. F. Dunbar, A. R. Buckley and D. G. Lidzey, *Energy Environ. Sci.*, 2014, **7**, 2944.
- P. Docampo, J. M. Ball, M. Darwich, G. E. Eperon and H. J. Snaith, *Nat. Commun.*, 2013, **4**, 2761.
- H. Zhang, H. Azimi, Y. Hou, T. Ameri, T. Przybilla, E. Spiecker, M. Kraft, U. Scherf and C. J. Brabec, *Chem. Mater.*, 2014, **26**, 5190.
- J. Min, Z.-G. Zhang, Y. Hou, C. O. Ramirez Quiroz, T. Przybilla, C. Bronnbauer, F. Guo, K. Forberich, H. Azimi, T. Ameri, E. Spiecker, Y. Li and C. J. Brabec, *Chem. Mater.*, 2015, **27**, 227.
- C.-Y. Chang, Y.-C. Chang, W.-K. Huang, K.-T. Lee, A.-C. Cho and C.-C. Hsu, *Chem. Mater.*, 2015, **27**, 7119.
- F. X. Xie, D. Zhang, H. Su, X. Ren, K. S. Wong, M. Grätzel and W. C. H. Choy, *ACS Nano*, 2015, **9**, 639.
- C.-Y. Chang, K.-T. Lee, W.-K. Huang, H.-Y. Siao and Y.-C. Chang, *Chem. Mater.*, 2015, **27**, 5122.
- S.-I. Na, S.-S. Kim, J. Jo and D.-Y. Kim, *Adv. Mater.*, 2008, **20**, 4061.
- H. Zhou, Y. Zhang, C.-K. Mai, S. D. Collins, T.-Q. Nguyen, G. C. Bazan and A. J. Heeger, *Adv. Mater.*, 2014, **26**, 780.
- Y. Yamada, M. Endo, A. Wakamiya and Y. Kanemitsu, *J. Phys. Chem. Lett.*, 2015, **6**, 482.
- S. D. Stranks, G. E. Eperon, G. Grancini, C. Menelaou, M. J. P. Alcocer, T. Leijtens, L. M. Herz, A. Petrozza and H. J. Snaith, *Science*, 2013, **342**, 341.
- G. Xing, N. Mathews, S. Sun, S. S. Lim, Y. M. Lam, M. Grätzel, S. Mhaisalkar and T. C. Sum, *Science*, 2013, **342**, 344.
- H.-L. Yip and A. K. Y. Jen, *Energy Environ. Sci.*, 2012, **5**, 5994.
- Y. Shao, Z. Xiao, C. Bi, Y. Yuan and J. Huang, *Nat. Commun.*, 2014, **5**.
- N. J. Jeon, J. H. Noh, W. S. Yang, Y. C. Kim, S. Ryu, J. Seo and S. I. Seok, *Nature*, 2015, **517**, 476.
- S. Pang, H. Hu, J. Zhang, S. Lv, Y. Yu, F. Wei, T. Qin, H. Xu, Z. Liu and G. Cui, *Chem. Mater.*, 2014, **26**, 1485.
- W. Chen, Y. Wu, Y. Yue, J. Liu, W. Zhang, X. Yang, H. Chen, E. Bi, I. Ashraf, M. Grätzel and L. Han, *Science*, 2015, DOI: 10.1126/science.aad1015.
- D. Yang, Z. Yang, W. Qin, Y. Zhang, S. Liu and C. Li, *J. Mater. Chem. A*, 2015, **3**, 9401.
- M. R. Leyden, M. V. Lee, S. R. Raga and Y. Qi, *J. Mater. Chem. A*, 2015, **3**, 16097.
- G. Niu, X. Guo and L. Wang, *J. Mater. Chem. A*, 2015, **3**, 8970.
- D. Liu and T. L. Kelly, *Nat. Photon.*, 2014, **8**, 133.

**Table 1** Summary of the photovoltaic properties of MAPbI<sub>3</sub>-based devices. The values in parenthesis are for the best performing devices

Device	Interfacial layer	V <sub>oc</sub> [volt]	J <sub>sc</sub> [mA cm <sup>-2</sup> ]	FF [%]	PCE [%]
A <sup>a</sup>	PC <sub>61</sub> BM	0.46 ± 0.01 (0.47)	15.04 ± 0.76 (15.14)	35.57 ± 4.42 (42.60)	2.44 ± 0.32 (3.03)
B <sup>b</sup>	Doped PC <sub>61</sub> BM	1.00 ± 0.01 (1.01)	20.13 ± 0.66 (20.27)	75.53 ± 3.88 (78.75)	15.19 ± 0.47 (16.11)
C <sup>a</sup>	PC <sub>61</sub> BM/ZnO	0.96 ± 0.01 (0.95)	15.69 ± 1.01 (16.29)	61.01 ± 4.13 (66.13)	9.15 ± 0.62 (10.23)
D <sup>a</sup>	PC <sub>61</sub> BM/CTAB	0.96 ± 0.01 (0.97)	15.92 ± 1.23 (19.27)	75.08 ± 9.44 (70.16)	11.39 ± 1.15 (13.11)

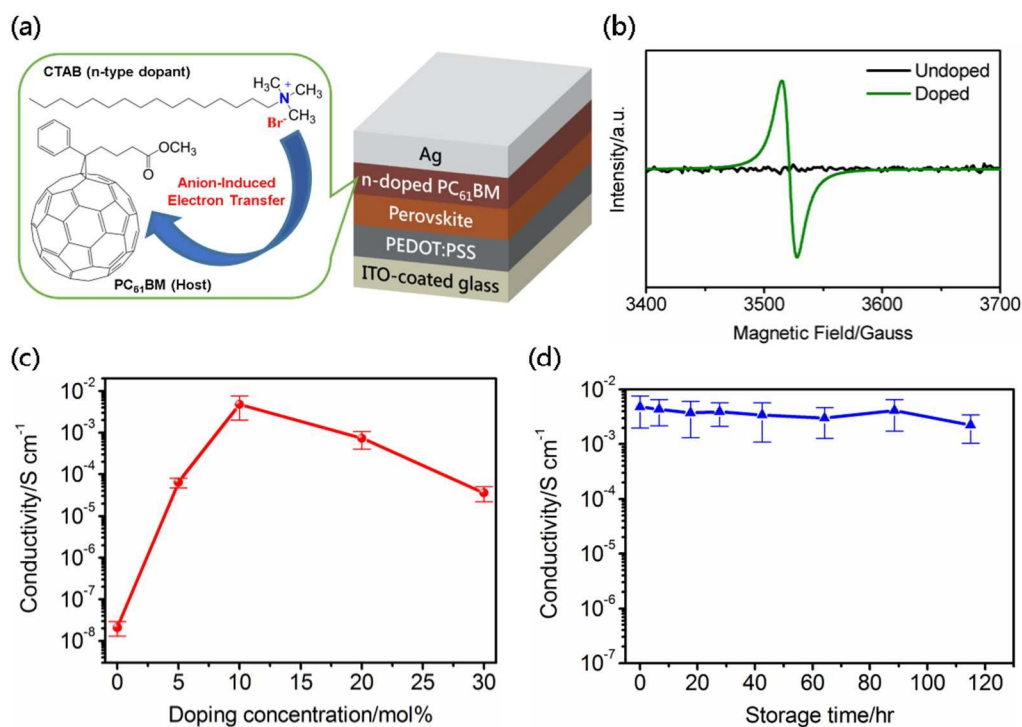
<sup>a</sup> Average and standard deviation values were obtained based on 30 devices.<sup>b</sup> Average and standard deviation values were obtained based on 50 devices.**Table 2** Summary of the photovoltaic properties of the best performing MAPbI<sub>3</sub>-based devices with various PC<sub>61</sub>BM thicknesses.

Interfacial layer	Thickness [nm]	V <sub>oc</sub> [volt]	J <sub>sc</sub> [mA cm <sup>-2</sup> ]	FF [%]	PCE [%]
PC <sub>61</sub> BM	60	0.47	15.14	42.60	3.03
PC <sub>61</sub> BM	80	0.47	14.20	31.68	2.11
Doped PC <sub>61</sub> BM	60	1.01	20.27	78.75	16.11
Doped PC <sub>61</sub> BM	80	1.03	20.22	72.34	15.07
Doped PC <sub>61</sub> BM	120	1.03	18.96	67.51	13.18

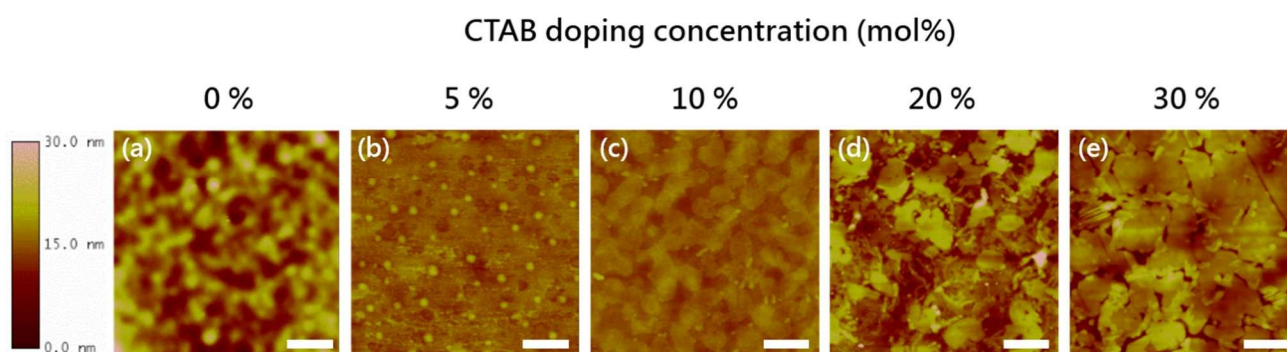
**Table 3** Summary of the photovoltaic properties of FAPbI<sub>3</sub>-based devices. The values in parenthesis are for the best performing devices

Device	Interfacial layer	V <sub>oc</sub> [volt]	J <sub>sc</sub> [mA cm <sup>-2</sup> ]	FF [%]	PCE [%]
E <sup>a</sup>	Doped PC <sub>61</sub> BM	1.00 ± 0.01 (1.01)	21.82 ± 0.94 (22.41)	71.73 ± 5.39 (75.60)	15.60 ± 0.75 (17.11)
F <sup>b</sup>	PC <sub>61</sub> BM	0.46 ± 0.01 (0.45)	15.59 ± 0.78 (16.28)	27.12 ± 1.76 (29.27)	1.94 ± 0.15 (2.15)
G <sup>b</sup>	PC <sub>61</sub> BM/ZnO	0.96 ± 0.01 (0.95)	16.32 ± 0.79 (17.55)	62.18 ± 4.05 (62.67)	9.68 ± 0.58 (10.45)

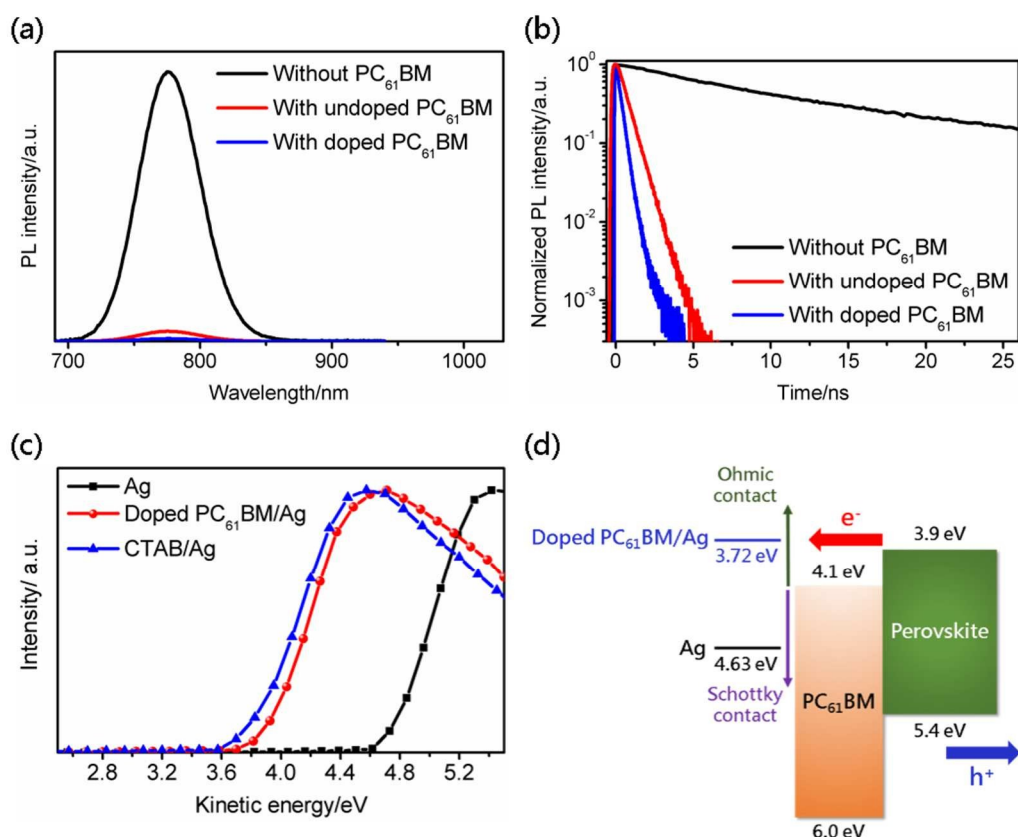
<sup>a</sup> Average and standard deviation values were obtained based on 30 devices.<sup>b</sup> Average and standard deviation values were obtained based on 10 devices.



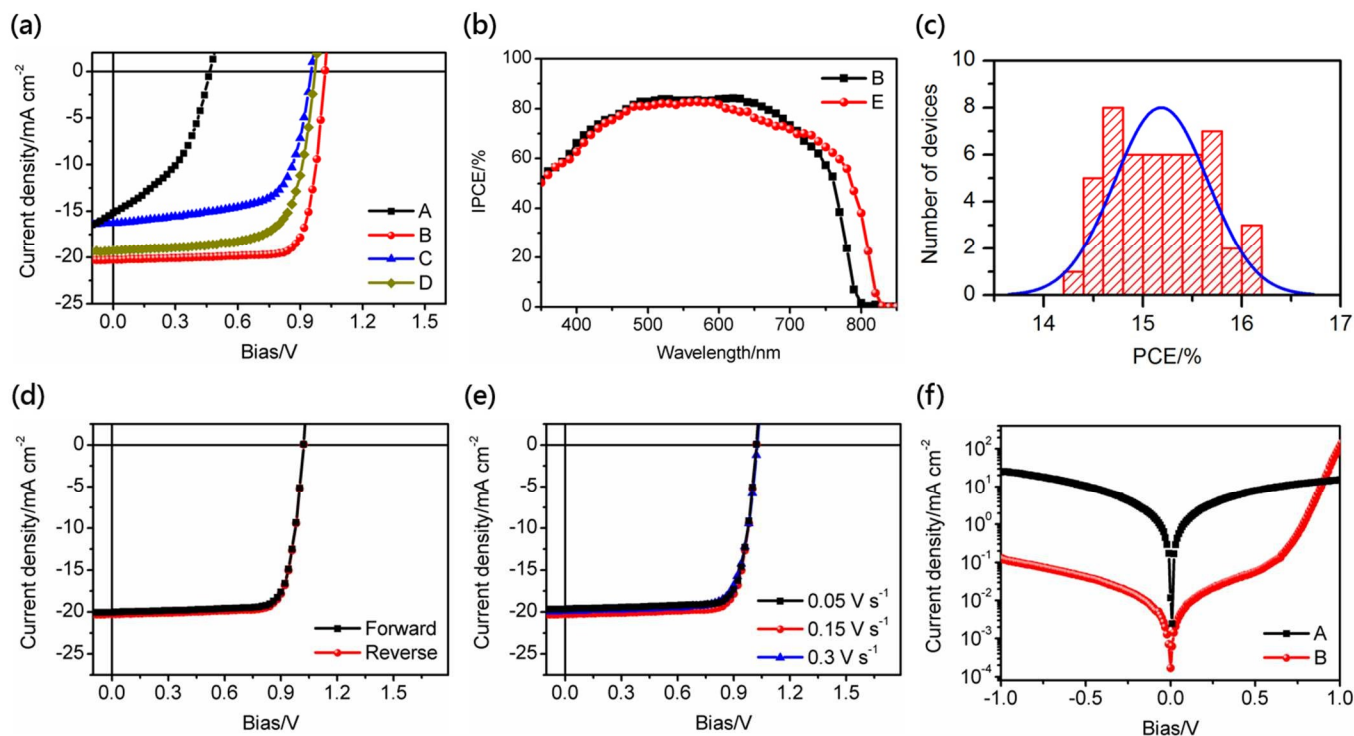
**Fig. 1** (a) Chemical structures of CTAB and PC<sub>61</sub>BM and a schematic illustration of the device architectures used in this study. (b) EPR spectra of the undoped PC<sub>61</sub>BM and CTAB-doped PC<sub>61</sub>BM in solid state. (c) Conductivities of CTAB-doped PC<sub>61</sub>BM films at varied dopant concentration. (d) Evolution of the conductivity of CTAB-doped PC<sub>61</sub>BM films (10 mol% doping) as a function of storage time in air. The statistical data were collected from more than 25 samples.



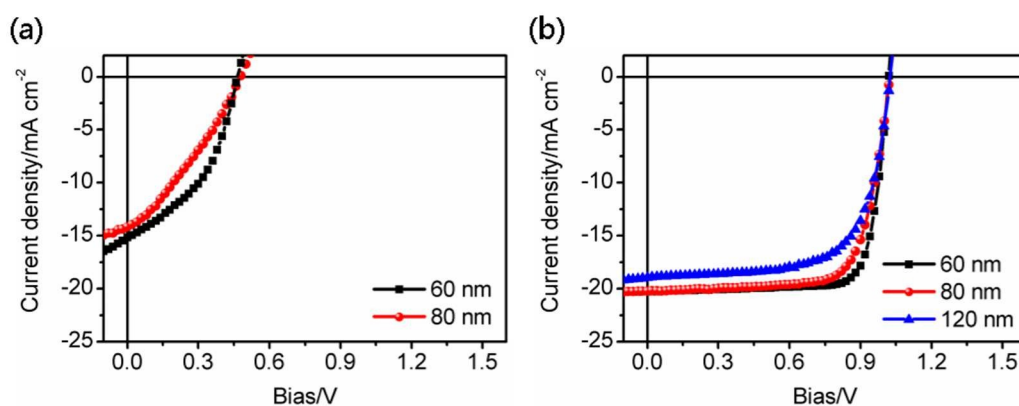
**Fig. 2** Topographical AFM images of CTAB-doped PC<sub>61</sub>BM films at varied dopant concentration (scale bar = 1 μm).



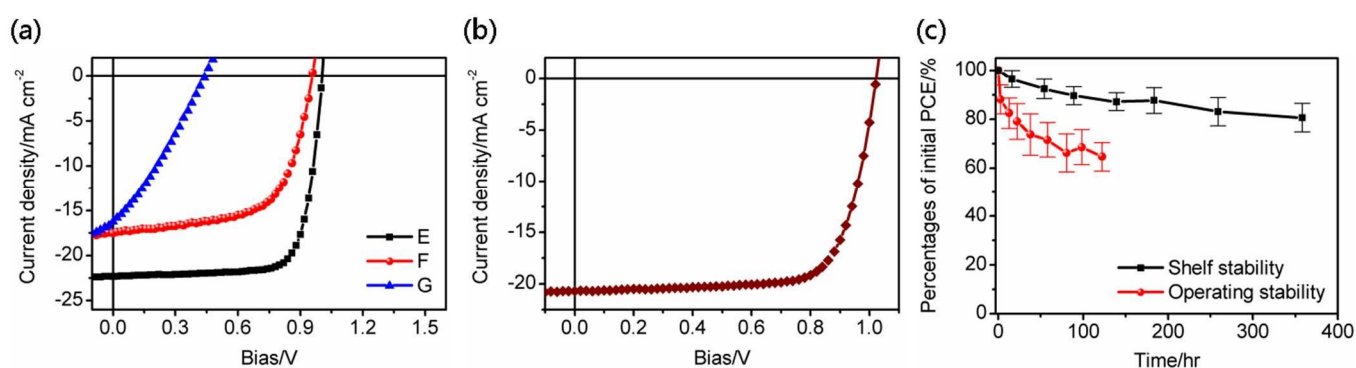
**Fig. 3** (a) Steady-state and (b) time-resolved PL spectra for MAPbI<sub>3</sub> films with and without PC<sub>61</sub>BM layers. (c) UPS spectra of bare Ag and modified Ag layers. (d) Energy level diagram at active layer/cathode interface.



**Fig. 4** (a) *J*-*V* characteristics of the best performing MAPbI<sub>3</sub>-based devices under simulated AM 1.5 solar irradiation. (b) IPCE spectra of the as-fabricated devices (Device B and E for MAPbI<sub>3</sub> and FAPbI<sub>3</sub> system, respectively). (c) Histogram of solar cell efficiencies (device B) for 50 devices. *J*-*V* characteristics of device B measured under simulated AM 1.5 solar irradiation with: (d) different sweep directions (scan rate = 0.15 V s<sup>-1</sup>) and (e) different voltage sweep rates. (f) Dark *J*-*V* characteristics of the as-fabricated devices.



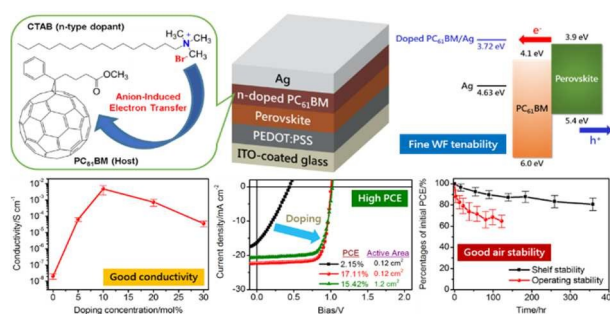
**Fig. 5** *J*-*V* characteristics of the best performing MAPbI<sub>3</sub>-based devices with various PC<sub>61</sub>BM thicknesses: (a) undoped film and (b) CTAB-doped film.



**Fig. 6** (a) *J*-*V* characteristics of the best performing FAPbI<sub>3</sub>-based devices (active area = 0.12 cm<sup>2</sup>) under simulated AM 1.5 solar irradiation. (b) *J*-*V* characteristics of the best performing FAPbI<sub>3</sub>-based devices (active area = 1.2 cm<sup>2</sup>) under simulated AM 1.5 solar irradiation. (c) Degradation profile of FAPbI<sub>3</sub>-based devices (active area = 1.2 cm<sup>2</sup>) as a function of storage time in ambient conditions (30 °C, ~60% relative humidity). The statistical data were collected from more than 10 devices.

## Graphical abstracts

## Solution-Processed n-Doped Fullerene Cathode Interfacial Layer for Efficient and Stable Large-Area Perovskite Solar Cells



**Highlight:** A facile and effective approach to enhance the performance and stability of perovskite solar cells is proposed by using solution-processed cetyltrimethylammonium bromide (CTAB)-doped [6,6]-phenyl-C<sub>61</sub>-butyric acid methyl ester (PC<sub>61</sub>BM) film as cathode interfacial layer.